CARBON 47 (2009) 2329–2336

available at www.sciencedirect.com

ScienceDirect

journal homepage: www.elsevier.com/locate/carbon

Small angle light scattering study of improved dispersion of carbon nanofibers in water by plasma treatment

Jian Zhao[a,b,c,*], *Donglu Shi*[b,d,e], *Jie Lian*[f]

[a]*The Key Laboratory of Rubber-Plastics (Qingdao University of Science and Technology), Ministry of Education, Qingdao 266042, China*
[b]*Department of Chemical and Materials Engineering, University of Cincinnati, Cincinnati, OH 45221-0012, USA*
[c]*Shandong University, Jinan 250061, China*
[d]*The Institute for Advanced Nanomaterials, Tongji University, Shanghai, China*
[e]*The Research Institute of Micro/Nano Science & Technology, Shanghai Jiaotong University, Shanghai 200240, China*
[f]*Department of Mechanical, Aerospace, and Nuclear Engineering, Rensselaer Polytechnic Institute, Troy, New York 12180, USA*

ARTICLE INFO

Article history:
Received 2 January 2009
Accepted 13 April 2009
Available online 22 April 2009

ABSTRACT

Ultrathin polymer film is deposited on the surfaces of vapor-grown carbon nanofibers by a plasma polymerization using acrylic acid as a monomer. Small angle light scattering is used to investigate the dispersion behavior of the carbon nanofibers suspended in water and provides information on the mechanism by which plasma treatment assists dispersion. Both plasma-treated and untreated nanofibers exhibit a hierarchical morphology consisting of small-scale aggregates that agglomerate to form fractal clusters that eventually precipitate. The time evolution of small-scale aggregation and large-scale agglomeration is studied by fitting the scattering data to a unified model. The morphology of the small-scale aggregates is also studied by extracting the size distribution from the angle-dependence of the scattered intensity, using the maximum entropy method in conjunction with a simplified tube form factor. The aggregates are side-by-side bundles of individual nanofibers or more complex structures. Plasma treatment not only contributes to breaking up of the small-scale aggregates into smaller sizes but also inhibits their agglomeration. For untreated fibers, large agglomerates appear immediately after sonication and their size remains almost unchanged during the precipitation process. For treated fibers, precipitation dominates during the first 8 h, leaving small entities in suspension which form agglomerates after a few days.
© 2009 Elsevier Ltd. All rights reserved.

1. Introduction

Carbon nanotubes are intrinsically one-dimensional structures that are chemically inert, and possess extraordinary mechanical and electronic properties [1,2]. Unfortunately, the advantages of carbon nanotubes have not been fully realized because the dispersion of carbon nanotubes is particularly intractable [3–6]. Although it is well known that plasma treatment modifies the surfaces of carbon nanotubes and thus improves the dispersion of carbon nanotubes, the measurement of the degree of dispersion remains challenging and the mechanism by which plasma treatment aids in the dispersion of carbon nanotubes is unknown. Here we use light scattering to quantify the dispersion of plasma-treated carbon nanofibers and elucidate their dispersion mechanism.

Deposition of a coating on carbon nanotubes could alter the surface properties of the nanotubes, offering a potential technological opportunity for improved dispersion. Plasma

* *Corresponding author*: Address: The Key Laboratory of Rubber-Plastics (Qingdao University of Science and Technology), Ministry of Education, No. 54, Zhengzhou Road, Qingdao 266042, China. Fax: +86 532 840 22924.
E-mail address: zhaojian@gmail.com (J. Zhao).
0008-6223/$ - see front matter © 2009 Elsevier Ltd. All rights reserved.
doi:10.1016/j.carbon.2009.04.023

polymerization has been used in surface and interface engineering for improving adhesion, hydrophobicity and hydrophilicity, corrosion resistance, and surface etching [7]. Low-temperature plasma polymerization treatment, a room temperature and environmentally benign process, can be used for surface modification and thin film deposition on almost all substances. Deposition of ultrathin films of highly cross-linked polymers on the surface of carbon nanofibers (or nanotubes) by a plasma polymerization has been achieved [8,9]. However, the nature of the dispersed entities in various media and the evolution of the dispersed state under quiescent conditions following sonication are unknown.

Many types of carbon nanotubes exist and the terminology is not universal. Carbon nanofibers are similar to multiwalled carbon nanotubes, but the carbon nanofibers are larger in diameter and much lower in cost, thus making them more suitable to practical applications.

Scattering methods have recently been employed to provide structural information about nanotube morphology [10–14]. In this work, we use small angle light scattering to infer the morphology of the plasma-treated vapor-grown carbon nanofibers and quantify the state dispersion of as-received and plasma-treated carbon nanofibers in water as a function of time. In order to better understand the state of aggregation of the nanofibers, we also estimate the size distribution from the light scattering data using the maximum entropy method [15,16]. We use the Irena code developed by Ilavsky and Jemian to get the maximum entropy solution [17,18].

The time evolution of the scattering data show that plasma treatment not only inhibits large-scale agglomeration, but also contributes to the morphological change of the short-scale bundling of fibers.

These observations have significant implications regarding the use of plasma-treated carbon nanofibers as a reinforcing filler to enhance the mechanical properties of polymer composites. The dispersion of untreated carbon nanofibers in matrix polymers has proven difficult, and the resulting composites do not show the anticipated properties. After plasma treatment, the dispersion of nanofibers in polymer matrices is greatly enhanced, thus leading to improved mechanical properties [9]. Light scattering study of plasma-treated carbon nanofibers suspended in media provides a morphological basis for improved performance of plasma-treated nanofiber reinforced polymer composites. Our observation is in good agreement with experimental investigation for enhanced dispersion of plasma-treated nanofibers in polymer composites [9].

2. Experimental

The carbon nanotubes we used are vapor-grown carbon nanofibers or simply carbon nanofibers. Vapor-grown carbon fibers have larger diameters than carbon nanotubes. Details regarding the nanofibers are given by Koerner et al. [19]. The vapor-grown nanofibers were provided by Applied Sciences Inc. Cedarville, OH. Pyrograf®-III PR19LHT nanofibers are vapor grown and subsequently heated to temperatures up to 3000 °C. The Pyrograf®-III carbon nanofibers normally contain a few concentric cylinders but may also be nested truncated cones. Typically the cores are open.

The carbon nanofibers (PR19HT) are plasma-treated using acrylic acid as a monomer. The plasma-coating facility is a homemade system. The plasma reactor for thin film deposition of nanoparticles has been introduced previously. The plasma reactor for plasma treatment of carbon nanofibers consists mainly of a radio frequency source, glass vacuum chamber and press gage [7,20,21]. The vacuum chamber of the plasma reactor has a long Pyrex glass column about 80 cm in height and 6 cm in internal diameter. The powder was vigorously stirred at the bottom of the tube and thus the surface of particles can be continuously renewed and exposed to the plasma during the plasma polymerization processing. A magnetic bar was used to stir the powders. The gases and monomers were introduced from the gas inlet during the plasma cleaning treatment or plasma polymerization. Before the plasma treatment, the basic pressure was pumped down to less than 50 mtorr and then the carrier gas (such as argon) or monomer vapors were introduced into the reactor chamber. The operating pressure was adjusted by the gas/monomer mass flow rate. During the plasma polymerization processing, the input power was 20 W and the system pressure was 300 mtorr. The plasma treatment time was 10 min.

TEM samples were prepared by allowing a drop of nanofiber suspension to dry onto Cu grids with holy-carbon film. The high-resolution transmission electron microscopy (HRTEM) experiments were performed using a JEOL JEM 2010F electron microscope with a field emission source. The accelerating voltage was 200 kV.

The dispersion efficiency was determined using a small angle light scattering photometer–a Micromeritics Saturn Digitizer (www.micromeritics.com). The data are reported in reciprocal space as intensity vs. the magnitude of the scattering vector, q. Light scattering covers the regime 10^{-6} Å$^{-1} < q < 10^{-3}$ Å^{-1}, where $q = (4\pi \sin\theta)/\lambda$, θ being half the scattering angle, and λ being the wavelength of the radiation in the medium. This q range corresponds to length-scales ($\sim q^{-1}$) from 100 μm at low-q to 1000 Å (0.1 μm) at high q. Deionized water was used as background.

3. Results and discussion

The as-received PR19HT powder consists of loosely aggregated nanofibers. Some nanofibers are curved with open ends. A representative HRTEM image of the original Pyrograf®-III PR19HT (Fig. 1) shows the graphite structure with the interlayer spacing $d = 0.34$ nm. Their diameters range from 20 to 100 nm in TEM. No iron catalyst particles are found by TEM.

To enhance dispersion ability of carbon nanofibers in water, acrylic acid is selected as a monomer for plasma polymerization. Bright-field and high-resolution TEM images of the plasma-coated nanofibers are shown in Fig. 2. An ultrathin film amorphous layer can be clearly seen covering the surface of the carbon nanofibers. The thin film is uniform with a thickness of approximately 2–7 nm surrounding the entire nanofiber surface.

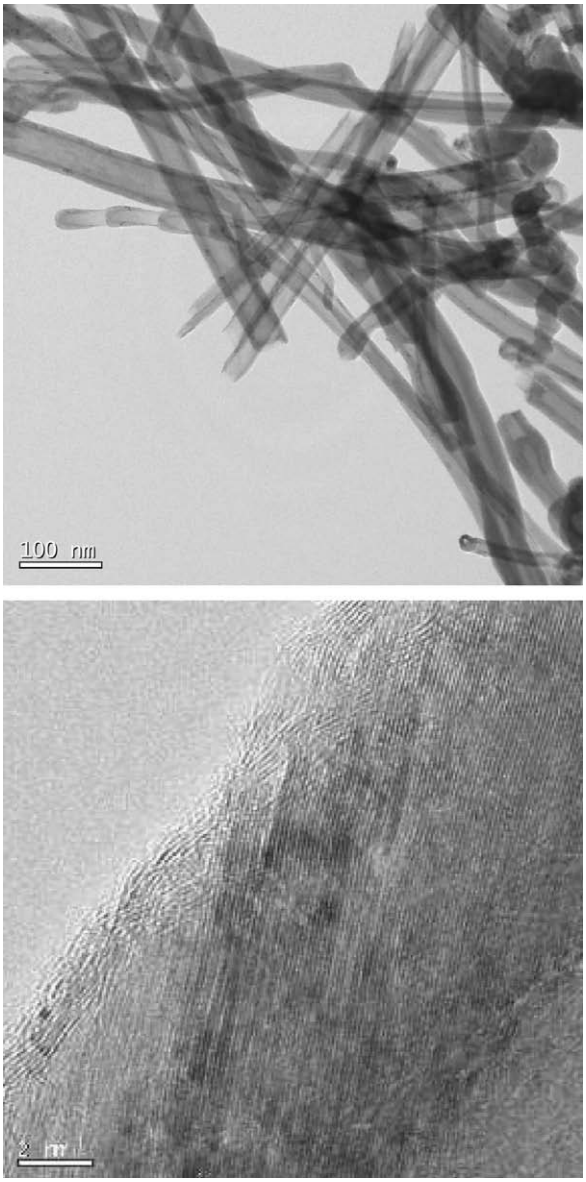

Fig. 1 – TEM images of unmodified carbon nanofibers PR19LHT. The low-resolution image shows a variety of tube shapes and morphologies including concentric cylinders and stacked cones. No metallic catalyst was observed. The bars are 2 nm and 100 nm.

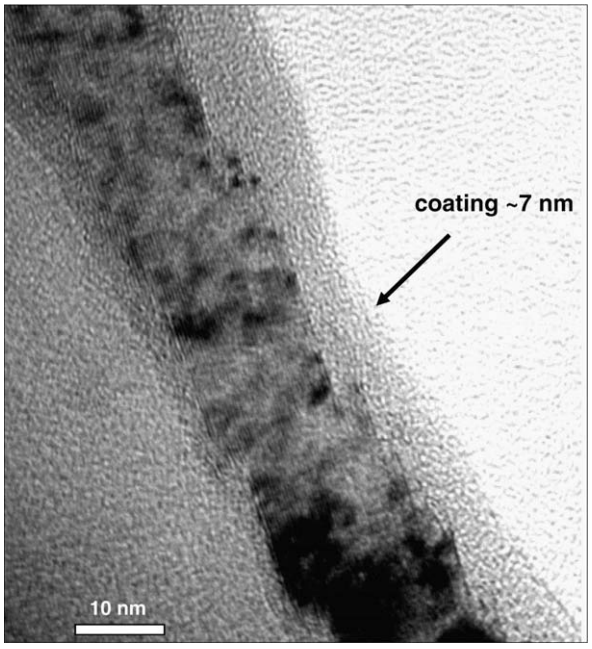

Fig. 2 – TEM image of plasma-treated carbon nanofibers PR19LHT: the bars are 10 nm. An ultrathin film of acrylic acid was observed on the surface of the nanofibers.

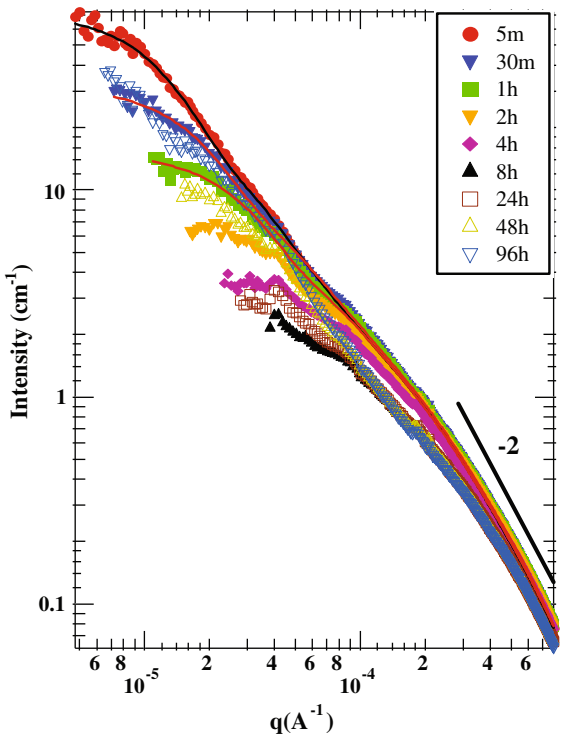

Fig. 3 – Evolution of the light scattering profile of plasma-treated nanofibers in water for four days following dispersion by sonication. The suspensions were sonicated at 10 W for 5 min before the observations began. The measurements were taken in the batch mode, so the sample was undisturbed during the course of the experiment. The lines are two-level unified fits. The unified parameters are collected in Table 1.

There is considerable experimental evidence for the presence of carboxylic acid functional group in an extremely thin layer of poly(acrylic acid) film [7,20]. The COOH on the coating could alter the surfaces of carbon nanofibers towards hydrophilicity and thus result in improved dispersion of carbon nanofibers in polar solvents. The coated carbon nanofibers are stable in water for weeks. In the absence of sonication, however, tubes aggregate and eventually precipitate. We use light scattering to monitor this process.

Fig. 3 shows the light scattering profiles as a function of time for plasma-treated nanofibers in water at a concentration of 5.0×10^{-6} g/ml. The data were obtained in the batch mode without agitation after the suspensions were sonicated at 10 W for 5 min. That is, the sample chamber was filled with

the undiluted suspension and observed without stirring, agitation or circulation. Deionized water was used as background.

Initially the scattered intensity at low-q drops with time. At 8 h, the maximal decrease in the intensity is observed. After 8 h, however, the intensity increases slowly, consistent with agglomeration. Substantial agglomeration is found after 48 h. In dilute solution the intensity at $q \to 0$ is proportional to molecular weight, so the data in Fig. 3 imply an increase of molecular weight by a factor of twenty between 8 and 96 h.

Although less visible for 4, 8 and 24 h data, the scattering curves consist of two power-law regimes and two Guinier regimes that define two "length scales". Each Guinier regime is followed by a quasi power-law regime. The curves were fit using Beaucage's Unified Model to extract radius of gyration Rg, the power-law exponents, P, and the Guinier prefactors, G, and power-law prefactor, B, associated with each length scale [22]. These parameters are displayed in Table 1 for the two structural levels. The slope near –2 ($P = 2$) on a log–log plot around $q = 0.002$ Å^{-1} could arise from a hollow tube since the wall of such an object is two-dimensional on scales larger than its wall thickness and shorter than the radius. Such a slope, however, can also arise from more complex aggregated structures [23]. The crossover length scale (q^{-1} 1 μm) between the two power-law regimes corresponds to the largest radius of the tube aggregates. Minimal change in Rg and P is observed for $q > 10^{-4}$ Å^{-1}, indicating minimal change in morphology with time on length scales below ~1 μm. Similar behavior was observed in the region $2 \times 10^{-4} < q < 2 \times 10^{-3}$ for single-walled nanotube suspensions [24].

The prefactor, G, extracted from high q structural level (level 1) decreases up to 8 h, indicating that the number and/or molecular weight of the small-scale entities is decreasing up to 8 h. After 48 h, however, the data indicate that these small-scale structure clusters form large-scale objects, which we call agglomerates. All the carbon precipitates after weeks.

We also studied dispersion behavior of untreated carbon nanofibers although such a suspension is quite unstable in water even with aid of ultrasound. The data for the untreated sample (Fig. 4) show similarities and differences when compared to the plasma-treated sample. Two structural levels are present and the length scales are similar to the plasma-treated case in Fig. 3. For the as-received sample, the large-scale agglomerates are observed immediately (5 min). The overall intensity shows a nearly monotonic, gradual decrease consistent with precipitation being the dominant process. The extracted Rgs are virtually unchanged during the precipitation process (Table 2). For the plasma-treated sample, the extracted Rgs are significantly smaller than those for untreated case. The plasma-treated nanofibers are suspended much longer than the untreated nanofibers. The size of the agglomerates dramatically decreases (Table 1) due to the presence of COOH groups on the surfaces of the coated carbon nanofibers.

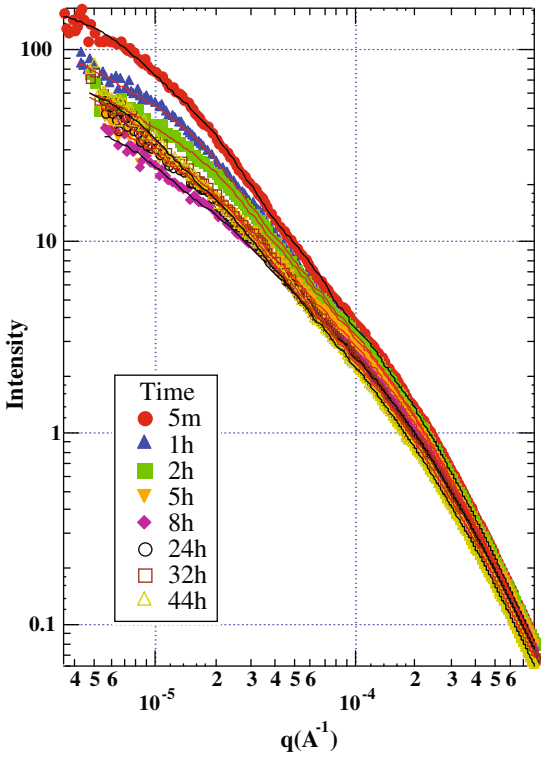

Fig. 4 – Evolution of the light scattering profile of unmodified nanofibers PR19HT for two days following dispersion by sonication. The suspensions were sonicated at 10 W for 5 min before the observations began. The measurements were taken in the batch mode, so the sample was undisturbed during the course of the experiment. The lines are two-level unified fits. The unified parameters are collected in Table 2.

Presumably, the number of the functional groups and the thickness of the plasma coating on the surface of nanofibers may vary, leading to difference in their dispersability. When they are suspended, larger agglomerates precipitate during the first 8 h, leaving smaller entities in suspension. After

Table 1 – Guinier radii and exponents as a function of time for plasma-treated carbon nanofibers.

	Time	5 min	30 min	1 h	2 h	4 h	8 h	24 h	48 h	96 h
Low-q	Rg (μm)	13.1	8.8	5.5	4.3	2.3	2.2	2.3	4.3	13.1
	P	1.58	1.43	1.39	1.22	1.21	1.20	1.20	1.47	1.70
	G	70.78	31.13	14.52	7.68	3.48	1.92	2.90	10.35	36.40
	106 B	70.31	3.26	4.41	21.87	13.81	10.84	15.50	1.47	17.06
High q	Rg (μm)	0.67	0.72	0.71	0.65	0.71	0.73	0.68	0.69	0.67
	P	1.93	2.07	1.90	1.97	1.97	1.90	1.95	1.94	2.10
	G	0.73	0.55	0.58	0.37	0.48	0.58	0.42	0.43	0.32
	108 B	6.58	1.14	11.34	5.69	5.67	29.6	5.55	4.92	1.64

Table 2 – Guinier radii and exponents as a function of time for as-received carbon nanofibers.

	Time	5 min	1 h	2 h	5 h	8 h	24 h	32 h	44 h
Low-q	Rg (μm)	21.3	20.9	20.8	19.4	18.6	19.5	20.1	20.2
	P	1.48	1.44	1.43	1.22	1.23	1.32	1.35	1.40
	G	160.2	110.1	74.2	51.5	44.9	65.2	70.1	74.3
	10^6 B	0.59	4.23	4.14	29.72	23.24	10.67	8.30	4.43
High q	Rg (μm)	0.86	0.84	0.88	0.83	0.87	0.83	0.83	0.82
	P	2.01	2.07	2.15	2.14	2.08	2.00	1.98	2.10
	G	1.53	1.24	1.46	0.92	1.00	0.67	0.66	0.69
	10^8 B	4.53	2.93	1.67	1.77	2.56	3.90	4.75	1.89

48 h, these small entities form large-structure agglomerates. After plasma treatment, the agglomerates are easier to break up and more difficult to grow. Plasma-treatment slows this agglomeration.

We compare the scattering profiles for plasma-treated and as-received carbon nanofibers at 8 h after sonication (Fig. 5). Compared to the untreated sample, the intensity at low-q (G) for the treated sample is one order of magnitude smaller, indicating small entities in the suspension. The extracted low-q Guinier radius is 2.2 μm for the plasma-treated sample, compared to 18.6 μm for the untreated case. These observations are consistent with improved dispersion due to the presence of the ultrathin plasma coating on the surface of the nanofibers.

The morphology of both the small and large-scale objects can be inferred from the power-law exponents, P, since P is the fractal dimension, D, of the objects giving rise to the scattering. $D = 1$ implies a linear object and $D > 1$ indicates more branched or flexible structures [12,23]. For our data, however, the scattering entities are polydisperse and the power-law regions extend over a very limited q range, so this approach is unworkable. An alternative is to use the relationship, $M_w \sim R_z^D$, where M_w is the weight-average molecular weight, R_z is the weight-squared-average radius and D is the fractal dimension of the object. Since $G \sim M_w$ and $R_z \sim R_g$, D can be extracted from the slope of a log–log plot of G vs. R_g. Such a plot is shown in Fig. 6 for the two structural levels for both the treated and untreated samples. Except for the low-q data for the treated sample, the data imply $D \geqslant 6$, which is unphysical. When the slope is greater than three we interpret the evolution of the scattering profile as due to precipitation of carbon nanofibers, because, to first approximation, G

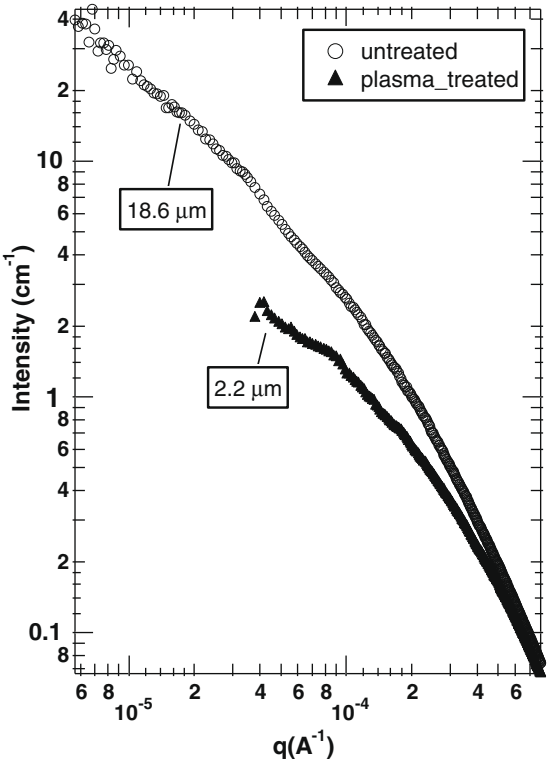

Fig. 5 – Comparison of the scattering profiles for untreated and plasma-treated carbon nanofibers 8 h after sonication. A substantial population of large-scale clusters is present only for the untreated sample.

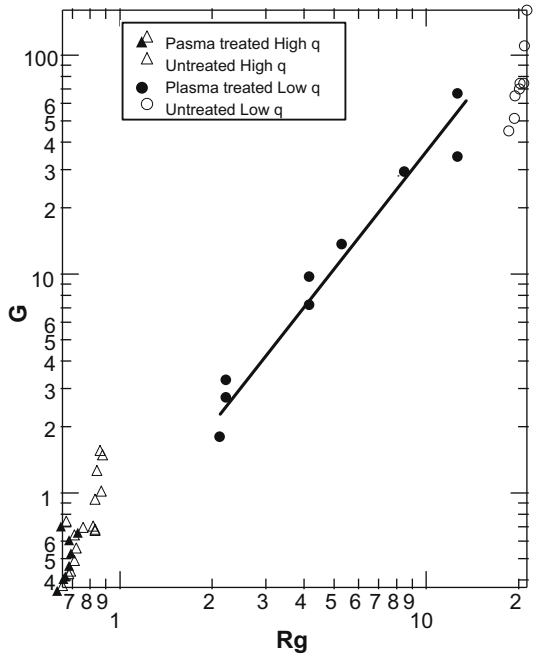

Fig. 6 – Relationship between the Guinier prefactors and the Guinier radius for two structural levels observed in Figs. 3 and 4. The low-q result for the treated sample is consistent with agglomeration to form a fractal cluster with fractal dimension $D = 1.7$. In the other cases, the large change in G with minimal change in R_g is consistent with sedimentation.

simply decreases at fixed R_g. For the untreated samples, therefore, both structural levels evolve by precipitation. For the plasma-treated sample, the small-scale objects precipitate for the first 8 h and then begin to agglomerate. The latter conclusion is reached because $D = 1.7 \pm 0.15$ for the large-scale structure (Fig. 6), consistent with a fractal morphology characteristic of agglomerates formed by kinetic growth. This number is also consistent with the value of P in Table 1 for the 96-h treated sample. For the other times, the power-law region is insufficient to compare the measured Ps and D from Fig. 6. For the plasma-treated sample, precipitation dominates agglomeration up to 8 h and agglomeration dominates precipitation after 8 h.

To further understand the morphology, the data were analyzed to determine the bundle size distributions using the maximum entropy method. To extract the size distribution a particle shape must be assumed. Electron microscopy shows that carbon nanofibers are more tube-like. The high q feature of the data should arise from this one-dimensional morphology.

As shown in Figs. 7 and 8, a tube model is investigated. Fig. 7 shows the fit to the light scattering data for the 8-h plasma-treated sample. Fig. 8 shows the corresponding volume distributions assuming a tube form factor with a wall thickness of 200 Å for 8-h untreated and plasma-treated samples. Actually, the position and shape of the distribution calculated for different tube-wall thicknesses do not show much difference (not shown here).

The model gives results with a peak in the diameter distribution around 0.52 μm for the 8-h untreated sample. The diameter at the peak is substantially larger than the tube diameters seen in TEM. The scattering entities are not individual tubes, but bundles. Both the peak position and the tails to larger sizes indicate that dispersion is not complete, based on the tube diameters seen in TEM. The bias to larger sizes is likely due to side-by-side fiber aggregates that are never disrupted.

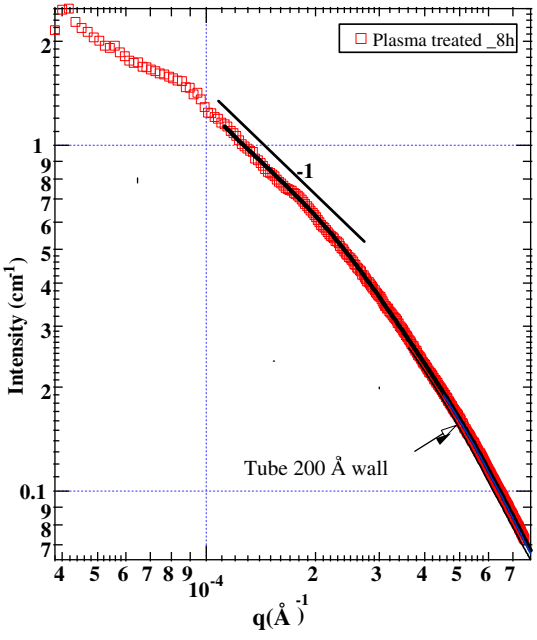

Fig. 7 – Maximum-entropy fits to the 8-h plasma-treated data assuming tubes with a wall thickness of 200 Å.

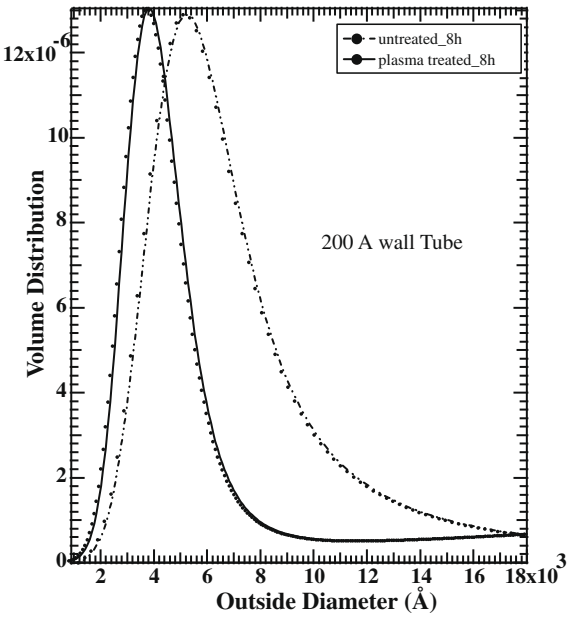

Fig. 8 – Comparison of volume distributions assuming tubes with a wall thickness of 200 Å for the 8-h untreated and plasma-treated data.

Comparison of the size distributions for untreated and plasma-treated samples (Fig. 8) shows that plasma treatment shifts the size distributions to smaller bundle sizes. That is, plasma treatment makes it easier to break up the aggregates. Since the contrast is not known, the volume distributions (ordinate in Fig. 8) are on an arbitrary scale. A peak in the diameter distribution for the plasma-treated sample shows up at around 0.38 μm, which is still larger than the largest individual fibers seen in TEM.

The simplified tube model used here was developed recently [25]. The simplified tube form factor approximates an exact tube model but suppress the oscillations that are found for exact models. This simplification is of minimal consequence when dealing with polydisperse distributions but it does accelerate the maximum entropy code.

We also compare Rgs derived from high q as a function of time for plasma-treated and untreated nanofibers (Fig. 9). In both cases, the Rgs (Fig. 9) extracted from these high q data show minimal change with time implying that the short-scale morphology is maintained during agglomeration and precipitation. Radius of gyration extracted from high q for plasma-treated sample is smaller than that for untreated sample (Fig. 9), consistent with the size distribution analysis. Plasma treatment assists in breaking up the larger aggregated structure into smaller bundles although aggregation still exists after plasma treatment. The dispersed bundles do not show further aggregation over time due to the presence of the ultra-thin plasma coating on the surfaces of carbon nanofibers.

Determining the size distribution for the low-q data is a challenge. In fact, we are not able to extract reasonable size distributions from the low-q portion data using a fractal aggregate model. The process of dispersion and precipitation,

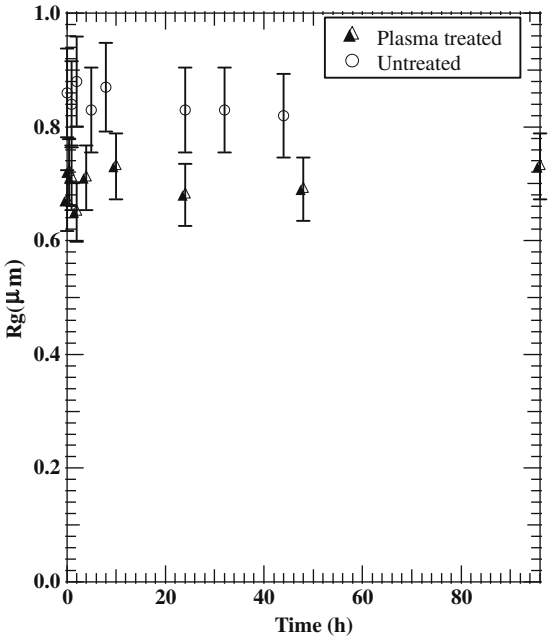

Fig. 9 – Radius-of-gyration (Rg) derived from high *q* region as a function of time for untreated and plasma-treated nanofibers. Error bars are also shown.

however, can be inferred from the time evolution of R_g and *G* extracted from the low-*q* unified fits. These parameters are found in Tables 1 and 2. Fig. 10a and b show R_g and *G* derived from low-*q* region as a function of time for plasma-treated and untreated nanofibers. For the untreated fibers, G decreases at nearly constant R_g, consistent with precipitation. After 8 h both R_g and *G* stabilize. For the plasma-treated case, *G* and R_g show a dramatic decrease up to 8 h consistent with sediment. Larger agglomerates precipitate, leaving smaller entities in the suspension. After 8 h, G and R_g increase with time consistent with agglomeration. It is interesting that these parameters tend to approach that of the untreated fibers. These observations are consistent with the fact that plasma treatment slows agglomeration and precipitation.

These results have significant implications for plasma-treated nanofibers as a reinforcing filler for polymer composites. Presumably, we are studying a more favorable dispersion environment compared to dispersion in polymers. For the latter case, there is a generic entropic barrier to dispersion of any colloid. When dispersed in polymers, it is reasonable that both untreated and plasma-treated carbon nanofibers still aggregate and agglomerate. Percolation thresholds are increased and mechanical properties are not those expected for a dispersion of isolated tubes. The reinforcing elements are disordered fractal objects (agglomerates). Such objects are unable to support even their own weight if they are too large. They behave as large voids that are responsible for decreasing composite moduli [9].

As stated in literature, the cluster size of plasma-treated nanofibers in polymer matrices is significantly reduced, [9] consistent with our observation that the plasma treatment suppresses agglomeration. The clusters correspond to fractal agglomerates studied in this paper. The smaller agglomerates after plasma treatment mitigate their void behavior and increase the interface area between the matrix and nanofibers, thus leading to considerably enhanced composite

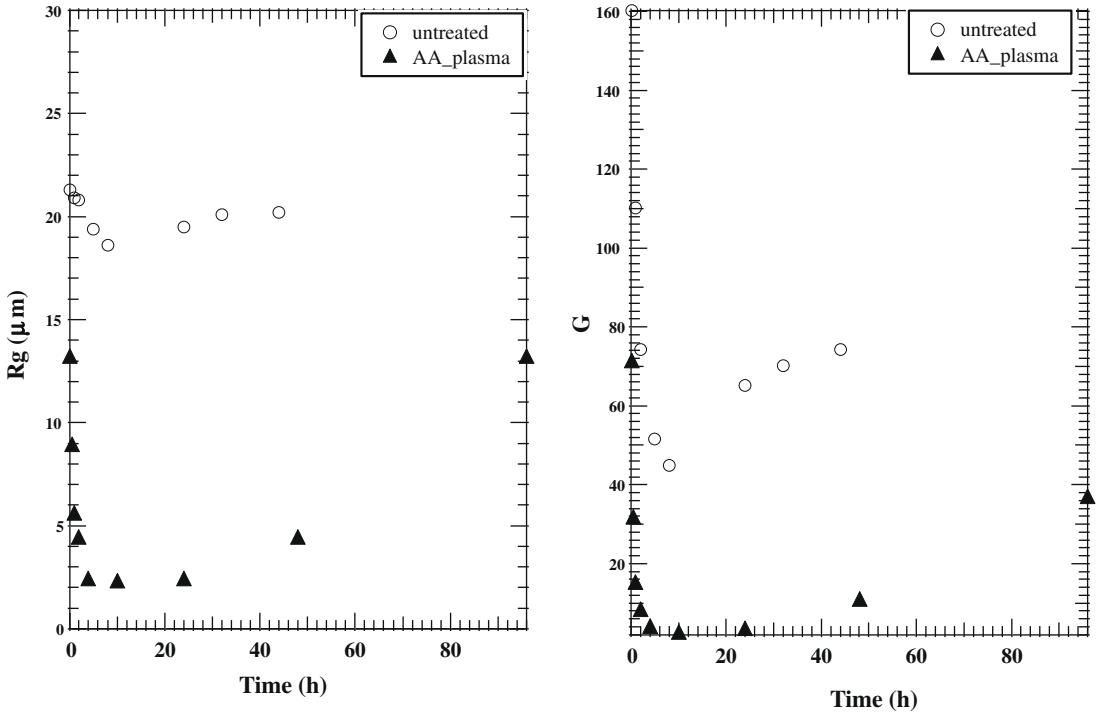

Fig. 10 – (a) Radius-of-gyration (Rg) derived from low-*q* region as a function of time for untreated and plasma-treated nanofibers. (b) G derived from low-*q* region as a function of time for untreated and plasma-treated nanofibers. At a given concentration G is proportional to the molecular weight.

performance. Although the morphology of the side-by-side aggregates of plasma-treated nanofibers in polymers is not studied in depth in literature, the presence of the plasma coating layer between carbon nanofibers and polymer matrices is obvious, contributing to enhanced load transfer between nanofibers and polymer matrices [9].

4. Conclusions

We compare dispersion behavior of plasma-treated and as-received carbon nanofibers suspended in water under quiescent conditions. Both samples show a hierarchical morphology consisting small-scale aggregates and large-scale agglomerates. The bundles consist of multiple fibers possibly aggregated side-by-side. In any case these objects agglomerate to form large-scale fractal clusters. Plasma treatment renders the small-scale aggregates smaller. In the absence of plasma treatment carbon nanofibers agglomerate immediately after sonication. In the plasma-treated case, for the first 8 h, precipitation is dominant, leaving small entities in solution. It takes days for the small objects to form agglomerates. Thus plasma treatment assists dispersion not only by inhibiting large-scale agglomeration but also by contributing to the morphological change of the small-scale aggregation of fibers. Ultimately, however, both treated and untreated fibers agglomerate to form fractal clusters that eventually precipitate. These observations are probably applicable to other plasma polymerizations and surface coatings when the resulting coating shows good compatibility with a solvent.

Acknowledgments

The authors are grateful to Professor Dale W. Schaefer and Gregory Beaucage (University of Cincinnati) for their valuable discussions in the light scattering experiments. The work was funded in part by the National Natural Science Foundation of China (No. 56776049 and 50603009), Doctoral Fund of Qingdao University of Science and Technology and the Key Laboratory of Rubber-Plastics (Qingdao University of Science and Technology), Ministry of Education, China.

REFERENCES

[1] Collins PG, Zettl A, Bando H, Thess A, Smalley RE. Nanotube nanodevices. Science 1997;278(5335):100–3.
[2] Dai LM, Mau AWH. Controlled synthesis and modification of carbon nanotubes and C-60: carbon nanostructures for advanced polymer composite materials. Adv Mater 2001;13(12–13):899–913.
[3] Hobbie EK, Wang H, Kim H, Han CC, Grulke EA, Obrzut J. Optical measurements of structure and orientation in sheared carbon-nanotube suspensions. Rev Sci Instrum 2002;74(3):1244–50.
[4] Shaffer MSP, Fan X, Windle AH. Dispersion and packing of carbon nanotubes. Carbon 1998;36(11):1603–12.
[5] Sandler J, Shaffer MSP, Prasse T, Bauhofer W, Schulte K, Windle AH. Development of a dispersion process for carbon nanotubes in an epoxy matrix and the resulting electrical properties. Polymer 1999;40(21):5967–71.
[6] Ajayan PM, Schadler LS, Giannaris C, Rubio A. Single-walled carbon nanotube-polymer composites: strength and weakness. Adv Mater 2000;12(10):750–5.
[7] Chityala A, van Ooij WJ. Surface modification of powders by plasma polymerization. Surf Eng 2000;16:299–308.
[8] Shi DL, Lian J, He P, Wang LM, van Ooij WJ, Schulz M, et al. Plasma deposition of Ultrathin polymer films on carbon nanotubes. Appl Phys Lett 2002;81(27):5216–8.
[9] Shi DL, Lian J, He P, Wang LM, Xiao F, Yang L, et al. Plasma coating of carbon nanofibers for enhanced dispersion and interfacial bonding in polymer composites. Appl Phys Lett 2003;83(25):5301–3.
[10] Bauer BJ, Hobbie EK, Becker ML. Small angle neutron scattering from labeled single wall carbon nanotubes. Macromolecules 2006;39:2637–42.
[11] Schaefer DW, Justice RS. How nano are nanocomposites? Macromolecules 2007;40(24):8501–17.
[12] Schaefer DW, Zhao J, Brown JM, Anderson DP, Tomlin DW. Morphology of dispersed carbon single-walled nanotubes. Chem Phys Lett 2003;375(3–4):369–75.
[13] Zhao C, Hu G, Justice R, Schaefer DW, Zhang S, Yang M, et al. Synthesis and characterization of multi-walled carbon nanotubes reinforced polyamide 6 via in situ polymerization. Polymer 2005;46(14):5125–32.
[14] Zhou W, Islam MF, Wang H, Ho D, Yodh AG, Winey KI, et al. Small angle neutron scattering from single wall carbon nanotube suspensions: evidence of isolated rigid rods and rod networks. Chem Phys Lett 2004;384:185–9.
[15] Morrison JD, Corcoran JD, Lewis KE. The determination of particle-size distributions in small-angle scattering using the maximum-entropy method. J Appl Crystallogr 1992;25:504–13.
[16] Potton JA, Daniell GJ, Rainford BD. Particle-size distributions from sans data using the maximum-entropy method. J Appl Crystallogr 1988;21:663–8.
[17] Ilavsky J. Particle size distribution from USAX, Irena SAS modeling macros manual. Argonne Illinois, USA: UNICAT; 2004.
[18] Jemian PR, Weertman JR, Long GG, Spal RD. Characterization of 9cr-1movnb steel by anomalous small-angle X-ray-scattering. Acta Metall Et Mater 1991;39(11):2477–87.
[19] Koerner H, Liu W, Alexander D, Mirau P, Dowty H, Vaia RA. Deformation-morphology correlations in electrically conductive carbon nanotube thermoplastic polyurethane nanocomposites. Polymer 2005;46:4405–20.
[20] Shi DL, He P, Lian J, Wang LM, van Ooij WJ. Plasma deposition and characterization of acrylic acid thin film on ZnO nanoparticles. J Mater Res 2002;17(10):2555–60.
[21] van Ooij WJ, Luo S, Zhang N, Chityala A. Surface engineering of powders and fibers by plasma techniques. In: Proceedings international conference on advanced Mfg technology. Xi'an, PR China, NY: Science Press; 1999. p. 1572–82.
[22] Beaucage G, Schaefer DW, Ulibarri T, Black E. Multiple size scale structures in silica siloxane composites studied by small-angle scattering. Abstr Pap Am Chem Soc 1994;207:144–9.
[23] Schaefer DW, Brown JM, Anderson DP, Zhao J, Chokalingam K, Tomlin D, et al. Structure and dispersion of carbon nanotubes. J Appl Crystallogr 2003;36:553–7.
[24] Chen Q, Saltiel C, Manickavasagam S, Schadler LS, Siegel RW, Yang H. Aggregation behavior of single-walled carbon nanotubes in dilute aqueous suspension. J Colloid Interf Sci 2004;280:91–7.
[25] Schaefer DW, Justice RS, Koerner H, Vaia R, Zhao C, Yang M, et al. Large-scale morphology of dispersed layered silicates. In: Pochan D, Bhatia SR, Khalifah PG, Radaelli P, editors. Neutron and X-ray scattering as probes of multiscale phenomena. Warrendale, PA: Materials Research Society 2005;840:Q3.3.1–3.3.6.